NANO LETTERS

LETTER

pubs.acs.org/NanoLett

Do Two-Dimensional "Noble Gas Atoms" Produce Molecular Honeycombs at a Metal Surface?

Jonathan Wyrick,[†] Dae-Ho Kim,[†] Dezheng Sun,[†] Zhihai Cheng,[†] Wenhao Lu,[†] Yeming Zhu,[†] Kristian Berland,[‡] Yong Su Kim,[§,∥] Eli Rotenberg,[§] Miaomiao Luo,[†] Per Hyldgaard,[‡] T. L. Einstein,[⊥] and Ludwig Bartels[*,†]

[†]Departments of Chemistry and Physics, University of California at Riverside, Riverside, California 92521, United States

[‡]Department of Microtechnology and Nanoscience, MC2, Chalmers University of Technology, SE-41296 Göteborg, Sweden

[§]Advanced Light Source, Lawrence Berkeley National Laboratory, Berkeley, California 94720, United States

[∥]Department of Applied Physics, Hanyang University, Ansan, Gyeonggi-do, 426-791, Korea

[⊥]Department of Physics, University of Maryland, College Park, Maryland 20742-4111, United States

Supporting Information

ABSTRACT: Anthraquinone self-assembles on Cu(111) into a giant honeycomb network with exactly three molecules on each side. Here we propose that the exceptional degree of order achieved in this system can be explained as a consequence of the confinement of substrate electrons in the pores, with the pore size tailored so that the confined electrons can adopt a noble-gas-like two-dimensional quasi-atom configuration with two filled shells. Formation of identical pores in a related adsorption system (at different overall periodicity due to the different molecule size) corroborates this concept. A combination of photoemission spectroscopy with density functional theory computations (including van der Waals interactions) of adsorbate–substrate interactions allows quantum mechanical modeling of the spectra of the resultant quasi-atoms and their energetics.

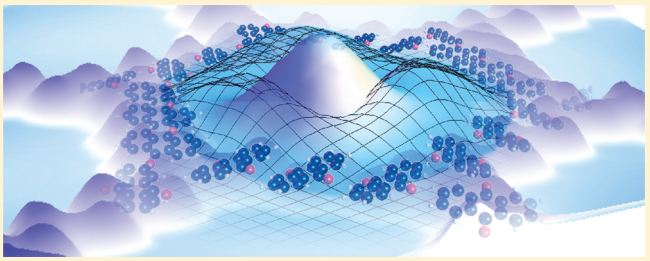

KEYWORDS: Quantum dots, molecular networks, self-assembly, scanning tunneling microscopy, adsorption at surfaces, Cu(111)

Since Eigler's group and others imaged the surface state oscillations on (111) surfaces of coinage metals[1−3] and showed that they can be confined in corrals set up from adsorbed atoms or molecules[4−7] two decades ago, their aesthetic appeal and fundamental physics have captivated the general public and surface scientists alike. In the meantime, evidence has been found that surface state scattering mediates interadsorbate interactions that favor particular separations or atomic patterns.[8−22] Here we show results that arguably close the circle begun with the formation of quantum corrals: the self-assembly of molecules into a regular porous network driven by optimization of the electronic quantum dot character of the surface state inside the pore. Thus, we find that quantum corrals, originally painstakingly assembled one atom at a time, can self-assemble in a molecular system driven by optimization of the quantum dot character of the enclosed electrons. While the effect of confinement on electronic states has been noted often, the idea that closed-shell "noble-gas"-like configurations have greater stability represents a new ordering principle in surface science. Molecular pores at surfaces can in turn serve to elucidate fundamental physics of adsorbates in confinement, as shown in refs 23−25.

Anthraquinone (AQ) molecules adsorb on Cu(111) into a molecular network that spans pores of ∼4 nm in diameter (Figure 1a). This network is stable up to ∼190 K. Underlying the formation of AQ chains and pinwheel vertices are attractive, short-range hydrogen bonds, which were measured to be ∼50 meV,[26] i.e., ∼100 meV per AQ–AQ bond; a very crude quantum chemical calculation gave a number of the same magnitude.[28,5] When we originally encountered this network,[19] we ascribed its formation to a competition between these attractions and an unspecified long-range force preventing aggregation into a compact pattern. Strikingly, this network is not only open but also very regular (the Supporting Information shows a portion of a network island consisting of 146 regular pores, with the only irregular ones (7) located at the island edge), suggesting that the effect causing pore formation favors one specific pore shape and size (a regular hexagon with three molecules per side): pores that have more or fewer than three molecules on any of their sides are typically present only to accommodate molecules pinned at surface defects such as step edges. A possible explanation of the observed size makes use of the oscillatory interaction mediated by the surface state on Cu(111),[27] which is much longer range than the analogous interaction mediated by bulk states,[20,28−30] Monte Carlo simulations based on this perspective in a simplified

Received: April 30, 2011
Revised: June 14, 2011
Published: June 15, 2011

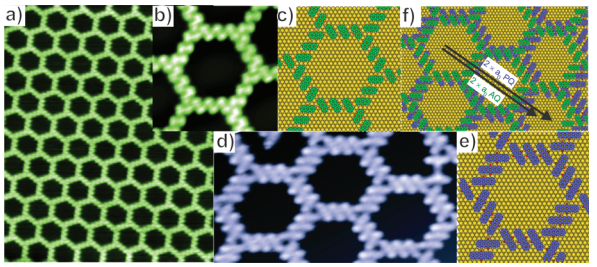

Figure 1. (a) STM image of regular AQ network. Image parameters: 26 nm × 29 nm; bias −2.53 V; current 0.05 nA. (b, c) Single pore of AQ (image parameters: 7.4 nm × 7.4 nm; bias −2.4 V; current 0.08 nA) and corresponding model. (d, e) PQ pores (image parameters: 19 nm × 9 nm; bias −3.8 V; current 0.01 nA) and corresponding model. (f) Superposition of PQ and AQ networks. The arrows show that the periodicities of the AQ and PQ networks differ substantially but their pore sizes are the same.

model could account generically for some of the experimental observations but were not fully satisfactory.[31] Also, at very low coverages only straight molecular rows are formed; virtually no vertices can be found suggesting that their presence is stabilized by the pore formation.

Lobo-Checa et al.[32] found that confinement of the surface state in a molecular network through scattering from organic molecules[33] can give rise to quantized electronic states, a concept further explored by Barth's group[34] and related to speculations about the stability of islands in metal epitaxy.[35] Given the high mobility of AQ on Cu(111),[26,36] we suggest that optimization of the electronic structure of the confined surface electrons, as 2D quantum dots with a closed-shell orbital configuration, is the foundation for the porous ordering of these films. In support of this proposition we find the formation of a network with virtually identical pores by substantially larger molecules (pentaquinone, PQ), requiring a different superlattice periodicity.

In this paper we present a combination of scanning tunneling microscopy (STM) and angle-resolved ultraviolet photoemission spectroscopy (ARUPS) data with theoretical modeling. All experiments use Cu(111) samples prepared by multiple sputtering and annealing cycles followed by deposition of AQ or PQ from a glass capillary. Synchrotron ARUPS experiments were conducted at beamline 7.0.1 of the Advanced Light Source using a gradient coverage created by gradually removing a shutter between deposition source and sample; STM experiments use homogeneous coverages. Deposition occurred on a cryogenic sample, and imaging proceeded after annealing to room temperatures. The modeling of the coupling between the molecular overlayer and the copper surface was based on density-functional theory (DFT) calculations using the PBE[37] functional with the ultrasoft pseudopotential code DACAPO[38] and including van der Waals interactions via the vdW-DF2 exchange-correlation functional.[39,40] The Supporting Information provides more detail.

In order to understand the effect of molecular network formation of AQ on the Cu(111) surface state, we model its confinement inside the pores not only for the experimentally observed pore geometry but also for all other pore shapes that can be created from AQ vertices and rows (even for pore shapes incompatible with continuous tiling of the surface). On the basis of the 3-fold symmetry of Cu(111), we begin with the eigenfunctions of a particle-in-a-triangular-box, which we relax into the pore boundary drawn by the locations of those AQ carbon and oxygen atoms

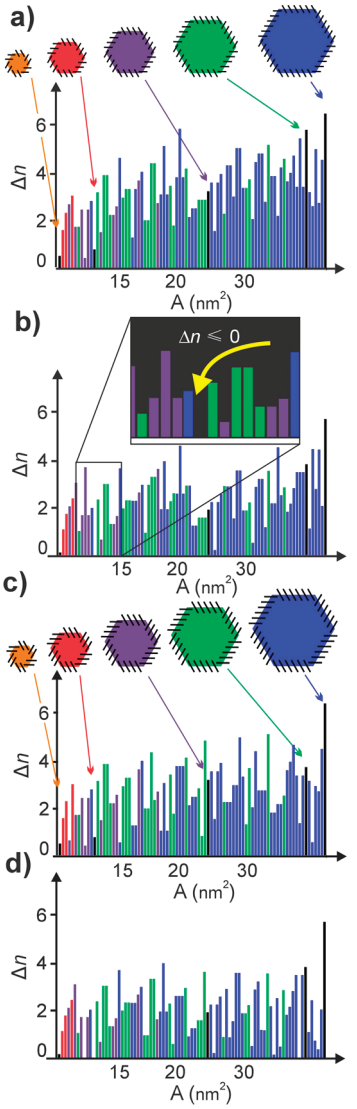

Figure 2. Graphs of electron deficit Δn for (a) AQ pores with no E_0 shift, (b) AQ pore with the experimentally determined E_0 shift included, and (c, d) equivalent plots for PQ. The pores are listed in order of increasing enclosed area, with regular hexagons shown in black. Colors indicate the number of molecules on the longest side of a given pore (mustard is 2, red is 3, purple is 4, green is 5, and blue is 6).

adjacent to the pore interior;[33] we find the resultant energy spectrum. The Supporting Information includes a table of the properties (spectrum, geometry, eigenstates, etc.) of the 85 pores considered; for reasons of practicality, we limit our survey to pores whose longest molecular row is 6 or fewer units long.

The Cu(111) surface state's band bottom E_0 (relative to the Fermi energy E_F) and its effective electron mass m have been established through ARUPS.[41,42] On a bare Cu(111) surface the surface state contains only a fraction γ of an electron per substrate atom, where

$$\gamma = \frac{m|E_0|A_0}{\pi\hbar^2}$$

with A_0 the area per atom on Cu(111); i.e., the surface state Fermi wave vector describes a circle much smaller than the surface Brillouin zone.

dx.doi.org/10.1021/nl201441b |*Nano Lett.* 2011, 11, 2944–2948

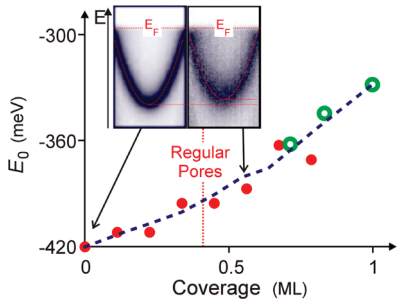

Figure 3. ARUPS measured coverage dependence of the surface state band bottom E_0 (red solid dots) and vdW-DF2 calculated coverage dependence of the surface state minimum (green hollow dots). A five-point average line is included to guide the eye. The inset shows the ARUPS spectra for the clean surface and for the coverage 0.56 monolayer, with 1 monolayer (ML) being the close-packed coverage and the vertical dotted line marking the coverage of the regular giant honeycomb network (Figure 1a). With increasing coverage the surface state band shifts up and loses spectral weight.

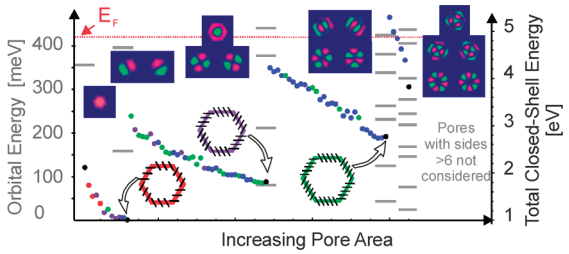

Figure 4. Electronic states (gray horizontal bars) of ideal hexagons with two to six AQs per side (left y axis, relative to E_0) and (for two AQs) their ground state and (for three to six AQs) their "valence" shell orbitals (i.e., first to fourth shell). The Supporting Information lists the spectra of all (not only the ideal hexagons) pores and all electronic states. The y axis on the right indicates the total electron energy, again referenced to E_0, required to fill all orbitals up to the "valence" shell for each of the possible AQ pores (same sequence and colors as in Figure 2a,b). Notably, the experimentally observed one has the lowest energy.

From the area enclosed by each pore, we can thus learn how many electrons the spectrum of the pore has to accommodate below E_F. Taking zero energy at our experimental surface state band bottom of −418 meV, we find that the electronic spectra of all possible pores have fewer levels below E_F than needed. Figure 2a plots this deficit (Δn) for all pores investigated in order of increasing pore area; it shows significant modulation since it depends on whether there are pore states just above or just below E_F. Again, all pores show an electron deficit.

Confinement of surface states is, however, not the only effect of AQ adsorption. In the simplest picture, AQ adsorption increases the surface dipole (due mainly to charge transfer to the more electronegative quinone), increasing the work function and shifting E_0 up (relative to E_F). We explored this phenomenon both experimentally by ARUPS and theoretically. Measuring the surface state dispersion on a sample as a function of the position in a gradient coverage, we find the position of the band bottom relative to E_F as a function of the coverage (Figure 3) similar to Scheybal et al.'s work on pentacene.[43] Unlike the molecular system of Lobo-Checa, et al.,[32] which can only assemble in one porous fashion, our ARUPS spectra do not show individual pore states, because several geometric factors prevent a dominant fraction of any crystal from being covered with a perfect AQ network (see discussion in Supporting Information). DFT modeling is only possible at or near the high coverage limit, because of the large slab thickness (at least six layers of Cu) required to model the surface state adequately. The green data points in Figure 3 correspond to calculations for parallel AQ rows separated by 0, 1, 2 substrate atomic spacings (3 × 5, 3 × 6, and 3 × 7 atoms supercells, see Supporting Information) and attach seamlessly to our experimental data set.

If the sole effect of AQ adsorption were the field due to the enhanced surface dipole, we would expect a linear dependence on coverage. This is qualitatively seen in Figure 3; to avoid prejudication of our model, we use a five-point-average fit to guide the eye; some nonlinearity is to be expected related to differences in the local geometries and sample quality.

Different-size pores correspond to different AQ coverages and, thus, different E_0. This, in turn, changes the fraction of the surface Brillouin zone corresponding to the occupied surface state and hence, γ, which becomes coverage/pore dependent. In this treatment we assume effects on m to be too small to be significant, supported by our theoretical modeling. As a consequence of the shift of E_0, Figure 2a needs to be rescaled, resulting in Figure 2b. Remarkably, the electron deficit Δn now vanishes for *one pore only*: the pore observed experimentally, i.e., a regular hexagon with three molecules per side. This invites the question: Why is this pore different from all other pores?

To answer this question, we turn to the properties of 2D quantum dots: in 1928 Fock solved the Schrödinger equation for a 2D quantum dot with noninteracting electrons confined by a quadratic potential, resulting in successive shells that can accommodate 2, 4, 6, 8, ... electrons (including 2-fold spin degeneracy).[44] Subsequently, it has been realized that this results in quantum dots with exceptional stability for magic numbers, N = 2, 6, 12, 20, ..., of electrons in filled-shell configurations (the equivalent of noble gases).[45,46] The lowest "orbital" corresponds to an orthogonal pair of simple harmonic oscillators (SHOs) both in the ground state $n_1 = n_2 = 0$, while the second orbital is doubly degenerate, with one SHO in $n = 0$ and the other in the first excited state $n = 1$; the third has either $n_1 = n_2 = 1$ or $n_{1,2} = 2$ and $n_{2,1} = 0$, etc. (Here we follow Fock's characterization in terms of two SHO quantum numbers $n_{1,2}$[44] rather than a principal and an orbital quantum number as in Darwin[47] and Kouwenhoven et al.[45,46])

Figure 4 shows on the left ordinate the spectrum of the regular AQ pores and for the smallest regular pore the ground state and for all other regular pores the "valence" shell orbital distribution. The states are not perfectly degenerate, as this would require 4-fold or circular symmetry, which is not achievable with the 0° or ±120° angles between adjacent molecules in the pore walls. Here the "valence" shell is the highest energy shell that is (at least partially) occupied to accommodate the number of surface state electrons originally present within the pore area. The local density of states of the orbitals of the experimentally observed pore has been confirmed by titration through CO adsorption, as recounted in refs 23 and 24.

We calculate the total energies, relative to E_0, of the electron distribution of each pore when filled up to a closed-shell noble-gas-like configuration and display them as dots referenced to the energy scale on the right ordinate of Figure 4. Remarkably, regular hexagons always have closed shells and have configurations at or near the lowest energy for each filled shell. Moreover, the experimentally observed pore geometry leads to the lowest overall energy of a closed shell (Figure 4). Thus, in summary,

dx.doi.org/10.1021/nl201441b |*Nano Lett.* 2011, 11, 2944–2948

regular AQ pores on Cu(111) match the size that leads to closed-shell 2D quantum dots, with nature choosing the pore that corresponds to the lowest energy closed-shell quantum dot. The dots are sufficiently large that two shells are filled, making the quasi-atom picture more compelling than in previous studies of laterally confined orbitals involving single orbitals.

Our evaluation uses no adjustable parameters and is robust with respect to small variations of the precise location of the surface state scattering and the shape of the E_0 fit curve (linear, square, five-point average). What we observe amounts to surface-state-driven formation of self-tailored quantum corrals. While the stabilization is not so large as to enable the formation of isolated pores in sparsely covered regions (where, instead, molecular rows form), it does provide an explanation for the surprising regularity of the cells given the high entropy associated with honeycomb cells in most physisorption systems.[48]

Since we could not directly observe these states in ARUPS, we provide an indirect corroboration that the pore size/shape and associated spectrum control the AQ self-assembly into a regular porous network: to this end, we sought and discovered a different adsorbate PQ with closely related substrate interactions (so that the E_0 vs coverage curve of Figure 3 is still valid) that assemble into pores with the same size/shape/spectrum as AQ although requiring a different lattice periodicity.

Deposition of PQ leads to a porous network on Cu(111) that does not quite exhibit the perfect ordering of AQ but which prominently features pores of virtually identical size and shape as AQ (Figure 1d−f). Given the larger size and higher aspect of the molecule, the vertex geometry is different from that of AQ and the overall periodicity of the PQ network is substantially larger (see superposition in Figure 1f). Due to the larger molecule body, PQ molecules are found to interact with one another in a larger variety of configurations leading to a far larger range of potential pore configurations. Evaluating PQ networks in the same manner as for AQ, we find that all pores have an electron deficit in the absence of the surface state band bottom shift (Figure 2c). However assuming the same coverage-E_0 shift relationship as for AQ (with 1 ML coverage being a smaller number density of molecules for PQ than AQ due to its larger size), we find that the pores of Figure 1d,e stand out as having no electron deficit (along with two others that do not tile and have a higher closed-shell energy). While the effect is not quite so striking for PQ as for AQ, it does corroborate the singular role of the pore shape/area adopted by AQ and its ability to drive network formation.

Our picture leads to a variety of predictions: if the network is indeed formed through coalescence of the surface state into quantum dots, then modifications of its properties using alkalis and halogens and (as Fock points out for the 2D SHO[44]) a magnetic field may pose an avenue to varying the surface pattern. Our description in terms of isolated 2D orbitals in each pore is the simplest possible; our DFT calculations suggest that in reality, some coupling between the pores, as envisioned by Lobo-Checa et al.[32] for smaller pores and narrower "walls", is likely to occur and should help stabilize the regularity of the giant honeycomb network. Readers familiar with semiconducting quantum dots may be concerned with the Coulomb repulsion between electrons in the pores, which scales with the reciprocal of the capacitance. On a metal surface, however, screening makes the capacitance enormous and the associated splitting negligible.

In conclusion, we have found not only that the surface state can be captured in quantum corrals but that the surface state itself can also be the driving force behind the formation of corrals that are minutely tailored to optimize the quantum dot character of its electronic setup, leading to coral shapes that are uniform across different adsorbate periodicities. Thus, what started as a survey of their aesthetics finally was realized to be a tool for surface patterning.

■ ASSOCIATED CONTENT

Supporting Information. Additional details of density functional work, why AQ pore states cannot be observed in ARUPS, and electronic states of AQ and PQ pores. This material is available free of charge via the Internet at http://pubs.acs.org.

■ AUTHOR INFORMATION

Corresponding Author
*E-mail: ludwig.bartels@ucr.edu.

■ ACKNOWLEDGMENT

We gratefully acknowledge joint support from NSF under Grants CHE 07-49949 (L.B.) and CHE 07-50334 (T.L.E.) and support from the Swedish Research Council (Vetenskapsrådet VR) under Grant No. 621-2008-4346. (P.H.) L.B. acknowledges additional support through DOE DE-FG02-07ER15842. T.L.E. acknowledges secondary support from NSF MRSEC Grant No. DMR 05-20471 and ancillary support from CNAM.

■ REFERENCES

(1) Hasegawa, Y.; Avouris, Ph. *Phys. Rev. Lett.* **1993**, *71*, 1071–1074.
(2) Crommie, M.; Lutz, C.; Eigler, D. *Nature* **1993**, *363*, 524–527.
(3) Li, J.; Schneider, W.; Berndt, R.; Crampin, S. *Phys. Rev. Lett.* **1998**, *80*, 3332–3335.
(4) Heller, E.; Crommie, M.; Lutz, C.; Eigler, D. *Nature* **1994**, *369*, 464–466.
(5) Li, J.; Schneider, W.; Crampin, S.; Berndt, R. *Surf. Sci.* **1999**, *422*, 95–106.
(6) Rieder, K.; Meyer, G.; Hla, S.; Moresco, F.; Braun, K.; Morgenstern, K.; Repp, J.; Foelsch, S.; Bartels, L. *Philos. Trans. R. Soc., A* **2004**, *362*, 1207–1216.
(7) Manoharan, H.; Lutz, C.; Eigler, D. *Nature* **2000**, *403*, 512–515.
(8) Silly, F.; Pivetta, M.; Ternes, M.; Patthey, F.; Pelz, J. P.; Schneider, W. D. *Phys. Rev. Lett.* **2004**, *92*, 016101.
(9) Repp, J.; Moresco, F.; Meyer, G.; Rieder, K.; Hyldgaard, P.; Persson, M. *Phys. Rev. Lett.* **2000**, *85*, 2981–2984.
(10) Stepanyuk, V.; Baranov, A.; Tsivlin, D.; Hergert, W.; Bruno, P.; Knorr, N.; Schneider, M.; Kern, K. *Phys. Rev. B* **2003**, *68*, 205410.
(11) Wong, K. L.; Rao, B. V.; Pawin, G.; Ulin-Avila, E.; Bartels, L. *J. Chem. Phys.* **2005**, *123*, 201102.
(12) Mitsui, T.; Rose, M. K.; Fomin, E.; Ogletree, D. F.; Salmeron, M. *Phys. Rev. Lett.* **2005**, *94*, 036101.
(13) Wang, Y. F.; Ge, X.; Manzano, C.; Korger, J.; Berndt, R.; Hofer, W. A.; Tang, H.; Cerda, J. *J. Am. Chem. Soc.* **2009**, *131*, 10400.
(14) Stranick, S. J.; Kamna, M. M.; Weiss, P. S. *Science* **1994**, *266*, 99–102.
(15) Kulawik, M.; Rust, H. P.; Heyde, M.; Nilius, N.; Mantooth, B. A.; Weiss, P. S.; Freund, H. J. *Surf. Sci.* **2005**, *590*, L253–L258.
(16) Sykes, E.; Han, P.; Kandel, S.; Kelly, K.; McCarty, G.; Weiss, P. *Acc. Chem. Res.* **2003**, *36*, 945–953.
(17) Nanayakkara, S. U.; Sykes, E. C. H.; Fernandez-Torres, L. C.; Blake, M. M.; Weiss, P. S. *Phys. Rev. Lett.* **2007**, *98*, 206108.
(18) Lukas, S.; Witte, G.; Woll, C. *Phys. Rev. Lett.* **2002**, *88*, 028301.
(19) Pawin, G.; Wong, K. L.; Kwon, K. Y.; Bartels, L. *Science* **2006**, *313*, 961–962.

(20) Einstein, T. L. Physical structure of solid surfaces. In *Handbook of surface science*; Unertl, W. N., Ed.; Elsevier: Amsterdam and New York, 1996; Vol. 1, pp 577−650.
(21) Fichthorn, K.; Scheffler, M. *Phys. Rev. Lett.* **2000**, *84*, 5371–5374.
(22) Österlund, L.; Pedersen, M.; Stensgaard, I.; Laesgaard, E.; Besenbacher, F. *Phys. Rev. Lett.* **1999**, *83*, 4812–4815.
(23) Cheng, Z.; Wyrick, J.; Luo, M.; Sun, D.; Kim, D.; Zhu, Y.; Lu, W.; Kim, K.; Einstein, T. L.; Bartels, L. *Phys. Rev. Lett.* **2010**, *105*, 066104.
(24) Cheng, Z.; Luo, M.; Wyrick, J.; Sun, D.; Kim, D.; Zhu, Y.; Lu, W.; Kim, K.; Einstein, T. L.; Bartels, L. *Nano Lett.* **2010**, *10*, 3700–3703.
(25) Kuehne, D.; Klappenberger, F.; Krenner, W.; Klyatskaya, S.; Ruben, M.; Barth, J. V. *Proc. Natl. Acad. Sci. U.S.A.* **2010**, *107*, 21332–21336.
(26) Pawin, G.; Solanki, U.; Kwon, K. Y.; Wong, K. L.; Lin, X.; Jiao, T.; Bartels, L. *J. Am. Chem. Soc.* **2007**, *129*, 12056–12057.
(27) Hyldgaard, P.; Einstein, T. L. *J. Cryst. Growth* **2005**, *275*, e1637–e1642.
(28) Tsong, T. T.; Casanova, R. *Phys. Rev. B* **1981**, *24*, 3063–3072.
(29) Kellogg, G. L. *Surf. Sci. Rep.* **1994**, *21*, 1–88.
(30) Fink, H. W.; Ehrlich, G. *J. Chem. Phys.* **1984**, *81*, 4657–4665.
(31) Kim, K.; Einstein, T. L. *Phys. Rev. B* **2011**in press.
(32) Lobo-Checa, J.; Matena, M.; Muller, K.; Dil, J. H.; Meier, F.; Gade, L. H.; Jung, T. A.; Stohr, M. *Science* **2009**, *325*, 300–303.
(33) Gross, L.; Moresco, F.; Savio, L.; Gourdon, A.; Joachim, C.; Rieder, K. *Phys. Rev. Lett.* **2004**, *93*, 056103.
(34) Klappenberger, F.; Kuhne, D.; Krenner, W.; Silanes, I.; Arnau, A.; de Abajo, F. J. G.; Klyatskaya, S.; Ruben, M.; Barth, J. V. *Phys. Rev. Lett.* **2011**, *106*, 026802.
(35) Morgenstern, K.; Laegsgaard, E.; Besenbacher, F. *Phys. Rev. Lett.* **2005**, *94*, 166104.
(36) Wong, K. L.; Pawin, G.; Kwon, K. Y.; Lin, X.; Jiao, T.; Fawcett, R.; Solanki, U.; Bartels, L.; Stolbov, S.; Rahman, T. S. *Science* **2007**, *315*, 1391–1393.
(37) Perdew, J. P.; Burke, K.; Ernzerhof, M. *Phys. Rev. Lett.* **1996**, *77*, 3865–3868.
(38) Dacapo Website: http://www.camp.dtu.dk/software.aspx/Dacapo/.
(39) Lee, K.; Murray, E. D.; Kong, L. Z.; Lundqvist, B. I.; Langreth, D. C. *Phys. Rev. B* **2010**, *82*, 081101.
(40) Dion, M.; Rydberg, H.; Schröder, E.; Langreth, D. C.; Lundqvist, B. I. *Phys. Rev. Lett.* **2004**, *92*, 246401.
(41) Fiete, G. A.; Heller, E. J. *Rev. Mod. Phys.* **2003**, *75*, 933–948.
(42) Kevan, S. D.; Gaylord, R. H. *Phys. Rev. B* **1987**, *36*, 5809–5818.
(43) Scheybal, A.; Muller, K.; Bertschinger, R.; Wahl, M.; Bendounan, A.; Aebi, P.; Jung, T. A. *Phys. Rev. B* **2009**, *79*, 115406.
(44) Fock, V. *Z. Phys.* **1928**, *47*, 446–448.
(45) Kouwenhoven, L.; Marcus, C. *Phys. World* **1998**, *11*, 35–39.
(46) Kouwenhoven, L. P.; Austing, D. G.; Tarucha, S. *Rep. Prog. Phys.* **2001**, *64*, 701–736.
(47) Darwin, C. G. *Proc. Cambridge Philos. Soc.* **1930**, *27*, 86–90.
(48) Villain, J. In *Ordering in strongly fluctuating condensed matter systems*; Riste, T., Ed.; Plenum Press: New York, 1980; pp 221−260.

Do 2D "Noble Gas Atoms" Produce Molecular Honeycombs at a Metal Surface?

Jonathan Wyrick,[1] Dae-Ho Kim,[1] Dezheng Sun,[1] Zhihai Cheng,[1] Wenhao Lu,[1] Yeming Zhu,[1]
Kristian Berland,[2] Yong Su Kim,[3,4] Eli Rotenberg,[3]
Miaomiao Luo,[1] Per Hyldgaard,[2]
*T. L. Einstein,[5] Ludwig Bartels[1]**

1. Departments of Chemistry and Physics, University of California at Riverside, Riverside, CA 92521, USA
2. Department of Microtechnology and Nanoscience, MC2, Chalmers University of Technology, SE-41296 Göteborg, Sweden
3. Advanced Light Source, Lawrence Berkeley National Laboratory, Berkeley, CA 94720, USA
4. Department of Applied Physics, Hanyang University, Ansan, Gyeonggi-do, 426-791, Korea
5. Department of Physics, University of Maryland, College Park, Maryland 20742-4111, USA

Supporting Information

A) Details of Density Functional Theory Work

The modeling of the coupling between the molecular overlayer and the copper surface is based on density-functional theory (DFT) calculations using the PBE functional [1] with the ultrasoft pseudopotential code DACAPO [2]. To consider the coverage dependence, we set up chains of AQs similar to the edges of the pores depicted in Fig. 1 in the manuscript, with different separations between the adjacent chains. Using periodic-boundary conditions and copper slabs six layers thick, topped by 18 Å of vacuum, we placed a single AQ molecule in 3×5, 3×6, and 3×7 unit cells of Cu(111) (Fig. S1 a,b,c respectively).

The height of the AQ above the substrate (3.55 Å) was set to that that of a para-benzoquinone molecule as determined in a non-self consistent vdW-DF2[3,4] calculation. A plane-wave energy cutoff of 400 eV, and corresponding density cutoff of 500 eV, and a 3×2×1 Brillouin zone sampling were used to obtain the electronic structure. Based on this result, the Kohn-Sham surface-state wave functions and eigenvalues at the $\overline{\Gamma}$ point were calculated separately for enhanced accuracy. In turn, the surface-state shift and wave-functions were extracted based on appropriate linear combinations of the Kohn-Sham orbitals[5].

We also note that the dependence of the effective mass on an applied field such as the dipole moment of adsorbates is found to be only ¼ of that of E_0, supporting the use of the simplifying assumption of an invariant surface state mass in the manuscript [5].

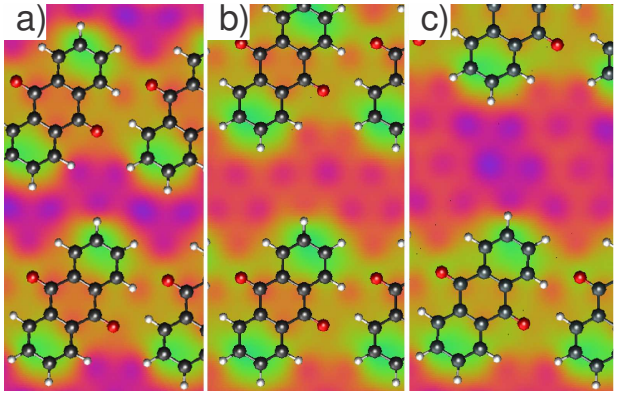

Fig. S1 Geometry used in modeling of the surface state band edge as a function of the coverage. Color coding represents the density of states of the surface state and reflects its reduction at the location of the molecules.

B) Why AQ pore states cannot be observed in ARUPS

At first glance, the model presented in the manuscript may appear to predict ARUPS spectra that show discrete AQ pore states. Ordered AQ networks are, however, best prepared on terraces which carry a substoichiometric coverage of AQ. Fig. S3a shows an example: the molecular network contains 146 regular pores on 4080 nm^2 terrace area; the coverage is 41% of the nominal AQ coverage of the regular network. At 9.6 nm^2 enclosed within each pore, this results in only 35 % of the surface area being the inside of regular pores.

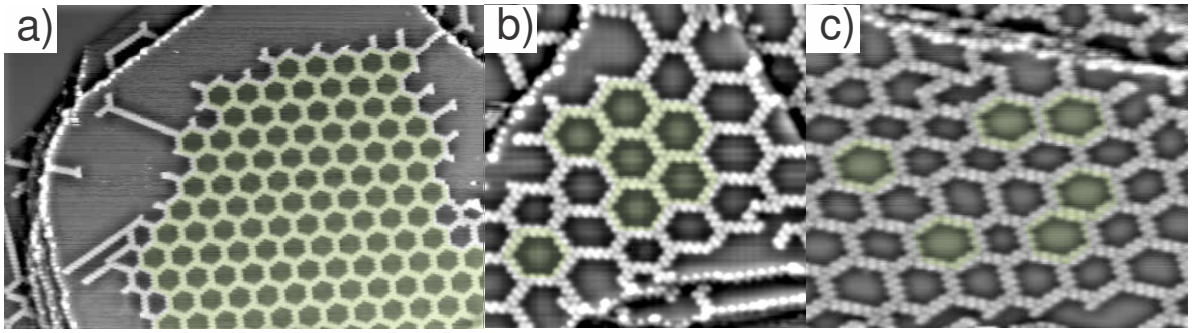

Figure S3 (a). Large Cu(111) terrace with regular AQ honeycomb at 41% coverage (image parameters: 85 nm × 57 nm; Bias –2.5 V; Current 0.05 nA). (b) Typical Cu(111) terrace with 7 regular honeycomb pores and many irregular pores caused by pinning at edges at a 78% of the nominal honeycomb coverage (image parameters: 27 nm × 27 nm; Bias –2.7 V; Current 0.1 nA (c) Largely irregular pore structure due to a small excess coverage (20%) of AQ on Cu(111) (image parameters: 31 nm × 18 nm; Bias –1.7 V; Current 0.1 nA).

If a larger coverage is chosen, AQ molecules pinned at kinks and step edges serve as the origin of AQ rows. If the AQ coverage is not significantly short of the optimal coverage, the network

will try to incorporate these rows by forming odd-shaped pores to accommodate their arbitrary origins. Consequently, a boundary of irregular pores surrounds a domain of regular pores on a terrace. Fig. S3b shows an array of pores on a 590 nm^2 terrace at a coverage of 78% of the nominal honecyomb coverage. In order to incorporate molecules pinned at step edges and kinks, numerous odd-shaped pores are necessary, resulting in only 6 central pores (and one towards the bottom left) being regular. Thus, the fraction of the surface area inside regular pores is 7x 9.6 nm^2/ 590 nm^2 = 11%.

If a slightly excessive coverage is used, the film will try to incorporate all AQ molecules in the network by creating smaller pores where necessary. Given the weak dependence of coverage on pore size, a large fraction of undersized pores are necessary to accommodate even a small excess coverage. These undersize pores, however, disrupt the overall film geometry, requiring further odd-shaped pores for their incorporation. This leads to a small fraction of regular pores on a surface, once optimal coverage is exceeded. Fig. S3c shows a terrace with a coverage of 120% of the nominal one of the honeycomb network. Clearly, many smaller-size pores are found, and only 13% of the surface area is covered with the interior of optimal pores.

Given the large area of each pore of 17 nm^2 (including the surrounding molecules), most terraces on our (typical) Cu(111) crystals are not wide enough to have many regular pores away from step edges. For surface-integrated ARUPS measurement, there is one more aggravating factor: while the area coverable with regular AQ pores scales linearly with terrace size, the area required to separate the film from step edges/kinks scales with the circumference of the terraces, i.e. the square root of the terrace area. Consequently, optimal coverage (including leaving space for the separation area) depends on the terrace size and, thus, can only be right in one preparation for one particular size (and shape) of terrace.

In combination, only a modest fraction of the average surface area will be covered with regular pores, explaining why ARUPS shows an average behavior of the surface state but no undispersed features or gaps, consistent with Fig. 3 of the manuscript. The ability to form pores of a large number of different sizes/shapes sets this system apart from the network investigated by Lobo-Checa[6] and, arguably, renders the formation of an ordered network an even more remarkable occurrence. The pores are also notably larger than those found by Klappenberger et al. [7], so that

more than one dot orbital is confined in the cell, as well as that observed by Silly et al.,[8] which has considerably more complicated geometry.

C) Electronic States of AQ and PQ Pores

Electronic spectra were calculated for all AQ and PQ pores possible for the nearest neighbor interactions shown in Fig. 1 of the manuscript irrespective of their ability to tile the surface. Calculations involve an iterative algorithm further described in Ref.[9]. An equivalent of Fig. 4 of the manuscript for PQ is shown for completeness below. The properties of PQ pores qualitatively resemble those of AQ pores. The two additional PQ pores of Fig. 2d with vanishing electron deficit have higher total energy than the experimental one, and their geometry does not lend itself to tiling of a surface.

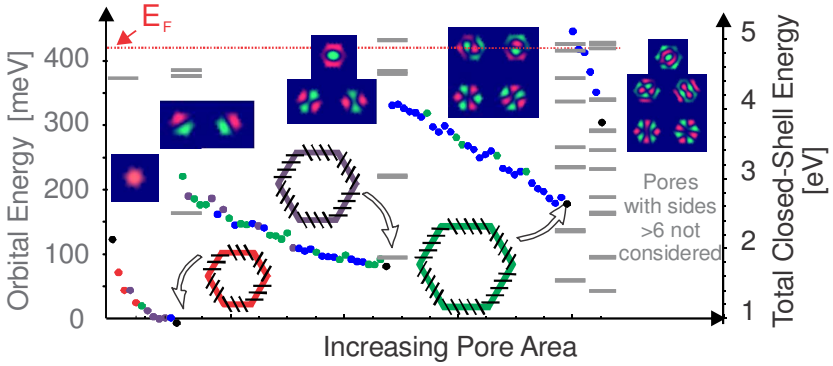

Fig. S2 Electronic states (grey bars) of ideal hexagons with 2-6 PQs per side (left y-axis, relative to E_0) and (for 2 AQ) their ground state and (for 3-6 AQ) their 'valence' shell orbitals (i.e. 1st-4th shell). Supporting Matierals Tables list the spectra of all (not only the ideal hexagons) pores and all electronic states. The y-axis on the right indicates the total electron energy, again referenced to E_0, required to fill all orbitals up to the 'valence' shell for each of the possible PQ pores (same sequence as in Fig. 2c,d). Notably, the experimentally observed one has the lowest energy.

Separate supporting information lists the electronic states of AQ and PQ for all pores addressed in the order of Figs. 2 & 4 of the manuscript, i.e. in order of increasing pore area. Electronic states that are within 10 meV from one another are drawn as degenerate for clarity in reference to solutions of the 2D harmonic oscillator with circular symmetry. Due to the difference between the vertex-to-vertex and side-to-side cross section of a hexagon, even the solutions for a perfectly-regular hexagon are not degenerate, in contrast e.g. to the phonon dispersion on a hexagonal lattice.

References

(1) Perdew, J. P.; Burke, K.; Ernzerhof, M. *Phys. Rev. Lett.* **1996**, *77*, 3865-3868.
(2)
(3) Lee, K.; Murray, E. D.; Kong, L. Z.; Lundqvist, B. I.; Langreth, D. C. *Phys. Rev. B* **2010**, *82*, 081101.
(4) Dion, M.; Rydberg, H.; Schröder, E.; Langreth, D. C.; Lundqvist, B. I. *Phys. Rev. Lett.* **2004**, *92*, 246401.
(5) Berland, K.; Hyldgaard, P.; Einstein, T. L. **in preparation**.
(6) Lobo-Checa, J.; Matena, M.; Muller, K.; Dil, J. H.; Meier, F.; Gade, L. H.; Jung, T. A.; Stohr, M. *Science* **2009**, *325*, 300-303.
(7) Klappenberger, F.; Kuhne, D.; Krenner, W.; Silanes, I.; Arnau, A.; de Abajo, F. J. G.; Klyatskaya, S.; Ruben, M.; Barth, J. V. *Phys. Rev. Lett.* **2011**, *106*, 026802
(8) Silly, F.; Pivetta, M.; Ternes, M.; Patthey, F.; Pelz, J. P.; Schneider, W. D. *Phys. Rev. Lett.* **2004**, *92*, 016101.
(9) Cheng, Z.; Wyrick, J.; Luo, M.; Sun, D.; Kim, D.; Zhu, Y.; Lu, W.; Kim, K.; Einstein, T. L.; Bartels, L. *Phys. Rev. Lett.* **2010**, *105*, 066104